

We are IntechOpen, the world's leading publisher of Open Access books Built by scientists, for scientists

6,900

Open access books available

185,000

International authors and editors

200M

Downloads

Our authors are among the

154

Countries delivered to

TOP 1%

most cited scientists

12.2%

Contributors from top 500 universities



WEB OF SCIENCE™

Selection of our books indexed in the Book Citation Index
in Web of Science™ Core Collection (BKCI)

Interested in publishing with us?
Contact book.department@intechopen.com

Numbers displayed above are based on latest data collected.
For more information visit www.intechopen.com



Designating Vulnerability of Atherosclerotic Plaques

Bukem Tanoren Bilen

Abstract

Microcalcification is an indication of vulnerability of plaques in humans. With conventional imaging modalities, screening of micrometer-sized structures in vivo with high spatial resolution has not been achieved. The goal of this study is to evaluate the potentials of micro-computed tomography (micro-CT), scanning electron microscopy (SEM), energy dispersive X-ray spectroscopy (EDS), time-resolved fluorescence spectroscopy (TRFS), scanning acoustic microscopy (SAM), and photoacoustic microscopy (PAM) in the determination of atherosclerotic plaques with microcalcifications and, therefore, the prospect of constructing a modality on a catheter system. The discrimination of microcalcifications within the fibrocalcific plaques and, therefore, the effectivity of these imaging techniques are discussed. The potential of quantum dots (QDs) in biological imaging is also elucidated since they attract great attention as contrast and therapeutic agents, owing unique properties including good light stability, low toxicity, strong fluorescence intensity, and changing emission wavelength with QD size, ranging from 10 to 100 Å in radius.

Keywords: atherosclerosis, vulnerable plaques, computed tomography, time-resolved fluorescence spectroscopy, scanning electron microscopy, scanning acoustic microscopy, photoacoustic microscopy, microcalcification, quantum dots

1. Introduction

Thin-cap fibroatheromas (TCFAs), which have fibrous caps of thickness of $<65\text{ }\mu\text{m}$ [1], are found to be at high risk for rupture. TCFAs have necrotic cores and also calcium depositions [2, 3]. Indicators of plaque vulnerability are microcalcifications or spotty calcifications within the plaques [4, 5], not larger calcifications, which are found to be stable and no longer threatening [6, 7]. Methods such as computed tomography (CT) and echocardiography, which are conventional noninvasive imaging modalities, can detect advanced calcifications. On the other hand, magnetic resonance imaging (MRI), micro-optical coherence tomography (micro-OCT) or positron emission tomography (PET) can identify early calcifications with limitations [6, 8]. However, these modalities are either very expensive or involve ionizing radiation. Therefore, seeking an alternative technique, which can give both morphological and chemical information about tissues at subcellular level, is inevitable.

Micro-CT is an accurate imaging modality for the observation of micrometer-sized structures, which can provide much higher resolution than cone beam computed tomography (CBCT) can. Quantitatively, micro-CT generally has a resolution of less than $10\text{ }\mu\text{m}$ voxel size, while CBCT has a resolution ranging between 76 and

400 μm [9–11]. Using X-rays, micro-CT can perform in vitro processing of the structure of materials such as composites, polymers, and biological materials (bone, teeth, cartilage tissue) and imaging of up to four different substances in a material [12] by a simple sample preparation and positioning procedure and without a requirement of high vacuum or low temperatures that may adversely affect the structure. However, micro-CT is an expensive diagnostic imaging technique requiring an ionizing radiation.

Scanning electron microscopy (SEM) can obtain images with a resolution in the order of a nanometer, by scanning the surface of the specimen with a focused beam of electrons. Energy dispersive X-ray spectroscopy (EDS), which can be implemented in electron microscope systems, is a chemical characterization technique detecting all elements ranging from beryllium (Be) to uranium (U) and their distributions within samples, also by the bombardment of the specimen surface with a focused electron beam. Consequently, both morphological and chemical information about the sample can be obtained by SEM-EDS. Microcalcifications can easily be observed with SEM-EDS; however, this would again be a very expensive method.

Time-resolved fluorescence spectroscopy (TRFS) measures the average fluorescence lifetime that a fluorophore spends in a biological tissue in the excited state, when it is excited by a source from its ground state, and the lifetime of the fluorophore changes as a result of interaction with its molecular environment. Various parameters regarding the molecular environment such as binding, temperature, or concentration can be analyzed by the change in the lifetime. TRFS has not been implemented in clinics yet, however, it has been investigated widely as a new tool for the characterization of atherosclerotic plaques. The success of TRFS in obtaining compositional information about the plaques [13–15] inspired scientists to combine fluorescence lifetime imaging with other modalities such as IVUS [16], second harmonic generation (SHG) microscopy [17], OCT [18], and Raman spectroscopy [19]. Intravascular catheters using TRFS technique have also been built [20, 21], since TRFS catheters can obtain good signals even within the artery, where blood does not affect lifetime properties but fluorescence intensity.

High axial and lateral resolutions of around 20–100 μm , a good penetration depth of around 5 mm, and low cost makes ultrasound imaging very popular for the observation of soft tissue; however, it can only provide morphological information. Besides, the signal detection capability of conventional ultrasonography has to be increased for the detection of microcalcifications, since high echo signals from such small surfaces are not available [22]. These disabilities have been overcome by combining ultrasound with photoacoustic imaging, and the detection of lipid-laden plaque was achieved by providing both morphological and lipid-specific chemical information about the human coronary artery [23]. Photoacoustic microscopy (PAM) is a well-known imaging modality that combines optical and ultrasound imaging. In this technique, typically, nanosecond lasers excite the tissue, and absorbed photons lead to pressure waves via thermoelastic expansion [24]. Ultrasonic transducers capture the emerged pressure waves and produce the map of optical absorbers located within the tissue. Since ultrasonic waves scatter less in biological tissue as opposed to visible portion of electromagnetic spectrum, whole body imaging is possible with a tomographic approach [25]. To increase the penetration even further, lasers operating in the near-infrared region are preferred for excitation where tissue is relatively transparent.

Scanning acoustic microscopy (SAM) is an imaging modality which gives information about the morphology and the mechanical properties of the specimen simultaneously at microscopic levels. High-frequency ultrasound signals are focused to identify the elastic properties of biological tissues. Major advantages of SAM over other imaging techniques are no requirement of special staining and

capture of an image of an area of around 5 mm x 5 mm in a couple of minutes. The speed of sound (SOS) through tissues [26–35] or acoustic impedance of samples [36, 37] can be calculated by SAM, and two-dimensional distributions are mapped. Similarly, cells and organelles can be resolved by acoustic microscopy using higher frequencies of 100–1200 MHz [38–45].

Quantum dots (QDs) are used as contrast and therapeutic agents since they have unique properties including strong fluorescence intensity with excellent light stability, low toxicity, and changing emission wavelength with QD size, ranging from 10 to 100 Å in radius [46]. Therefore, they possess great potential in the fields of biological imaging, molecular markers [47–49], and drug delivery [50–52]. QDs are useful in tumor detection [53], cardiovascular imaging [54], and cancer targeting [55]. Their high optical absorption and biocompatibility made noble metal nanoparticles to be widely used as biomarkers [56, 57]. On the other hand, graphene quantum dots (GQDs) are extensively used in biomedical applications [58, 59] since they exhibit lower cytotoxicity than cadmium (Cd), selenium (Se)-, and lead (Pb)-based quantum dots do [60]. The use of QDs as contrast agents in magnetic resonance imaging (MRI) [61], optical coherence tomography (OCT) [54], positron emission tomography (PET), single-photon emission computed tomography (SPECT), optical imaging such as fluorescence spectroscopy and Raman spectroscopy, and photoacoustic imaging (PAI) [62–64] proved their potential as diagnostic agents.

Here, we discuss the ability of these modalities in discriminating the collagen-rich areas from calcified regions within human carotid plaques. Micro-CT and SEM monitors microcalcifications, while EDS provides elemental distribution within plaques. TRFS provides information about the molecular environment of the plaques with the help of QDs. PAM is successful in imaging the fibrocalcific plaques with micrometer resolution. SAM provides micrometer resolution in morphology and also mechanical information about the samples, and therefore, differentiation of the collagen-rich areas from calcified regions is achieved.

2. Imaging of human fibrocalcific plaques

2.1 Micro-computed tomography (micro-CT)

Plaques fixed within 2% formaldehyde can be monitored with micro-CT, after obtaining micro-focal spot and arranging high-resolution detectors for X-rays. With full-scan mode 360° for each plaque, calcifications spread through are observed as can be seen in **Figure 1**.

2.2 Scanning electron microscopy and energy dispersive X-ray spectroscopy (SEM-EDS)

SEM images of the collagen-rich and calcified regions of the plaques can be obtained as shown in **Figure 2** and in **Figure 3**, respectively. EDS analyses of representative regions 2 and 3 are shown in **Figure 4** and in **Figure 5**, respectively. SEM images can be used to differentiate collagen-rich and calcific regions in fibrocalcific plaques, and EDS analyses are performed for determining the compositional differences between two regions of interest. In **Figure 2**, collagen-rich region in one plaque sample is observed and one region is chosen for EDS analysis. Similarly, in **Figure 3**, calcification-rich region is visualized in one sample and one region is chosen for EDS analysis. As can be seen in **Figure 4**, in collagen-rich regions, calcium deposition is insignificant, while in calcified regions, as shown in **Figure 5**, calcium peak is pronounced.

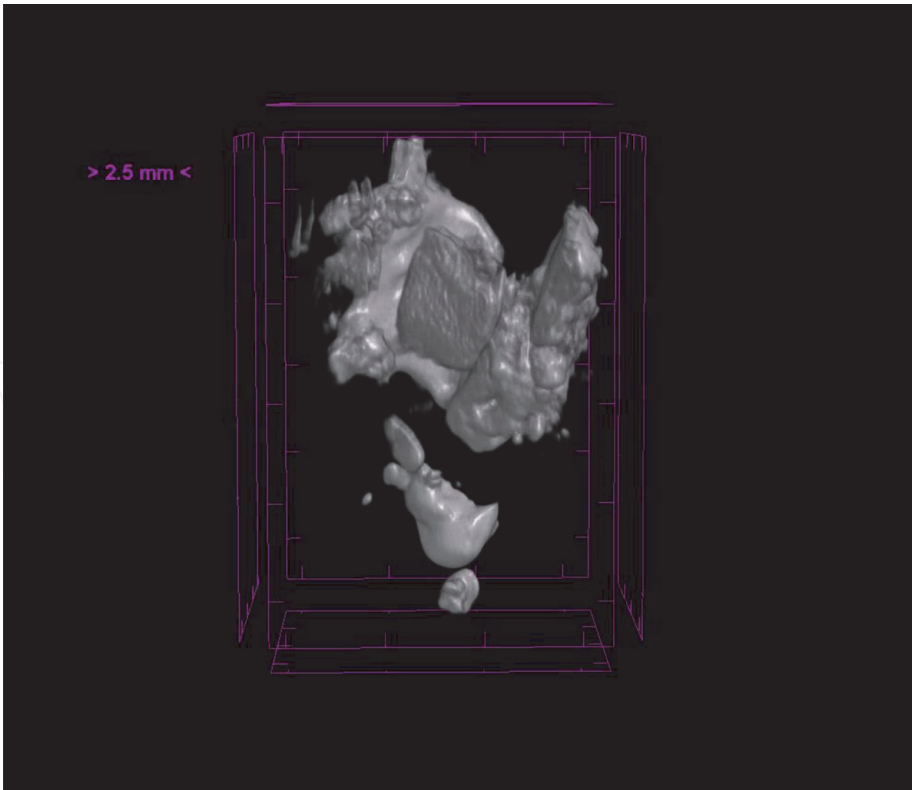


Figure 1.
Micro-CT image of a fibrocalcific plaque sample in which the calcifications can be monitored clearly in three dimensions.

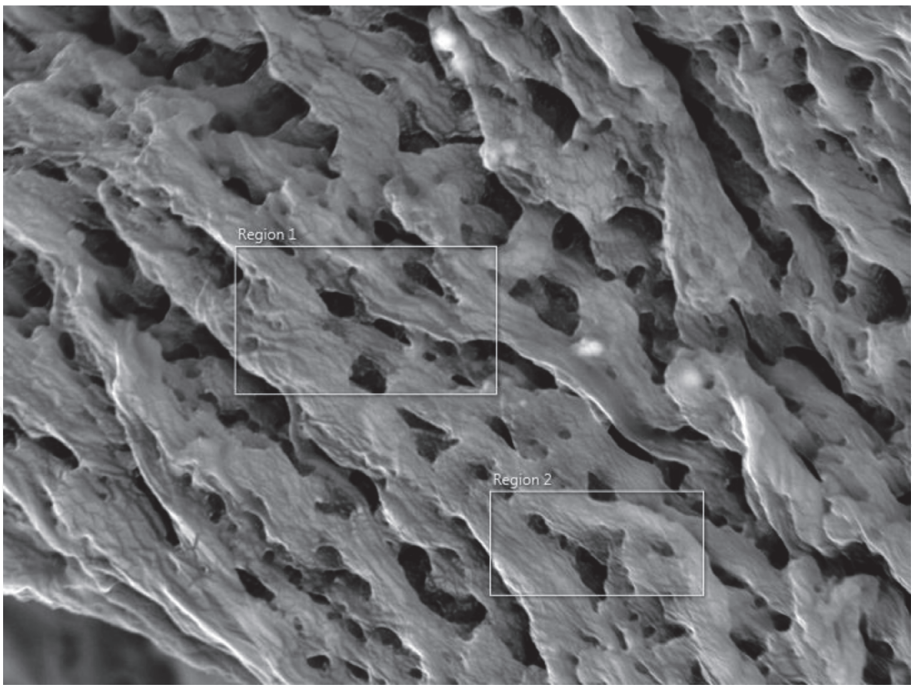


Figure 2.
Scanning electron microscopy image of the collagen-rich region of the plaque. Energy dispersive X-ray spectroscopy is performed on the designated region 2.

2.3 Time-resolved fluorescence spectroscopy (TRFS)

For TRFS experiments, cadmium-telluride/cadmium sulfide (CdTe/CdS) QDs are sprayed on plaque samples and fluorescence lifetimes of the QDs are determined.

The decay of the fluorescence intensity $I(t)$ at time t is given as

$$I(t) = \sum_{i=1}^n A_i \exp\left(\frac{-t}{\tau_i}\right) \tag{1}$$

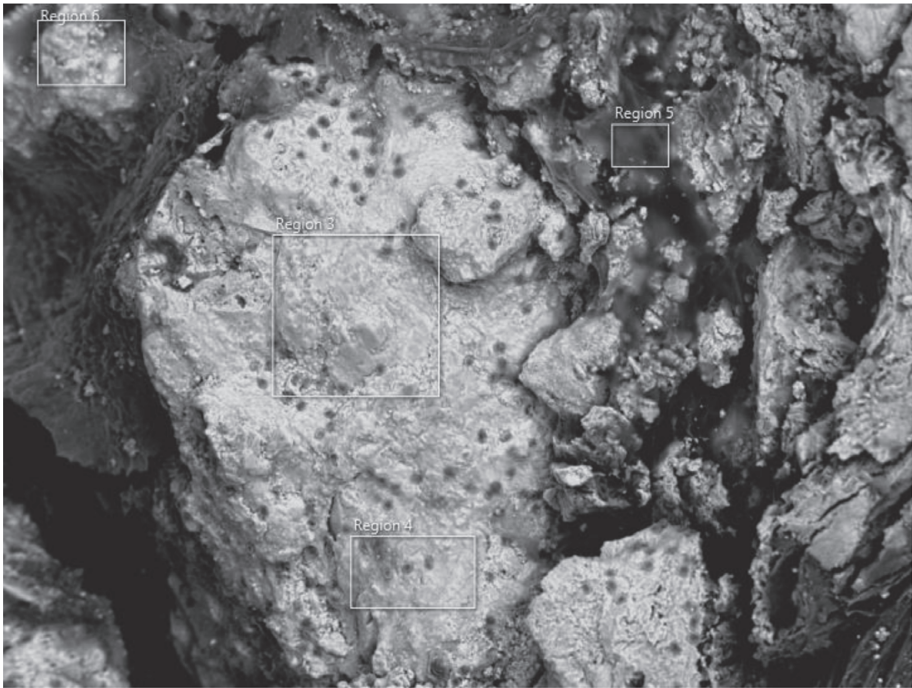


Figure 3.
Scanning electron microscopy image of the calcific region of the plaque. Energy dispersive X-ray spectroscopy is performed on the designated region 3.



Figure 4.
*Energy dispersive X-ray spectroscopy result of the highly calcified region 2, shown in **Figure 2**.*



Figure 5.
*Energy dispersive X-ray spectroscopy result of the highly calcified region 3, shown in **Figure 3**.*

where τ_i represents the fluorescence lifetime of the i th component and A_i is its corresponding decay amplitude. The fractional impact of the components to the total intensity is given by

$$f_i = \frac{A_i \tau_i}{\sum_i A_i \tau_i} \tag{2}$$

The intensity decay is evaluated using the average intensity lifetime or the average amplitude lifetime. The amplitude average lifetime is obtained from

$$\langle \tau \rangle = \sum_i f_i \tau_i \tag{3}$$

The intensity average lifetime is obtained from

$$\tau = \frac{\sum_i A_i \tau_i}{\sum_i A_i} \tag{4}$$

The fluorescence lifetime of QDs is measured on a microscope slide prior to the experiment for the comparison of the lifetime value with those measured on the plaque samples. The lifetime of the QDs on the microscope slide is measured to be 9.24 ns. As seen in **Table 1**, the fluorescence lifetime values of the QDs on a plaque sample are different on various regions.

Figure 6 shows the fluorescence lifetime decay curves acquired from the excitation of the CdTe/CdS QDs on the plaque sample for regions 1, 3, and 4. For the different regions of the sample, the parameters of the decay populations of the QDs confined on the plaque are determined by the two exponential decay fit, minimizing the χ^2 parameter. A significant change is noticeably seen in the characteristics of these three curves for various regions of the sample. These results clearly show that there is an obvious and efficient electron transfer between the QDs and the regions of the plaque, and therefore, there are noticeably different decay parameters at collagen-rich and calcified regions. TRFS is successful in providing information about the molecular environment of the plaque.

2.4 Scanning acoustic microscopy (SAM)

SAM images of the atherosclerotic plaques are received using acoustic impedance mode of SAM as can be seen in **Figure 7**. This image is constructed using the acoustic reflections from both surfaces of the reference (water) and the plaque cross

Region	τ_1 (ns)	τ_2 (ns)	$\langle \tau \rangle$ (ns)	$\langle \tau \rangle$ (ns)	χ^2
1	2.90	0.61	1.31	2.17	0.82
2	3.35	0.72	1.36	2.30	0.87
3	4.30	1.00	1.90	3.03	0.86
4	4.73	1.09	2.30	3.60	1.03
5	4.54	1.01	1.91	3.15	1.03
6	4.87	1.06	2.09	3.50	0.93
7	3.70	0.83	1.44	2.41	0.97

Table 1.
Fluorescence decay parameters of CdTe/CdS QDs on different regions of the plaque.

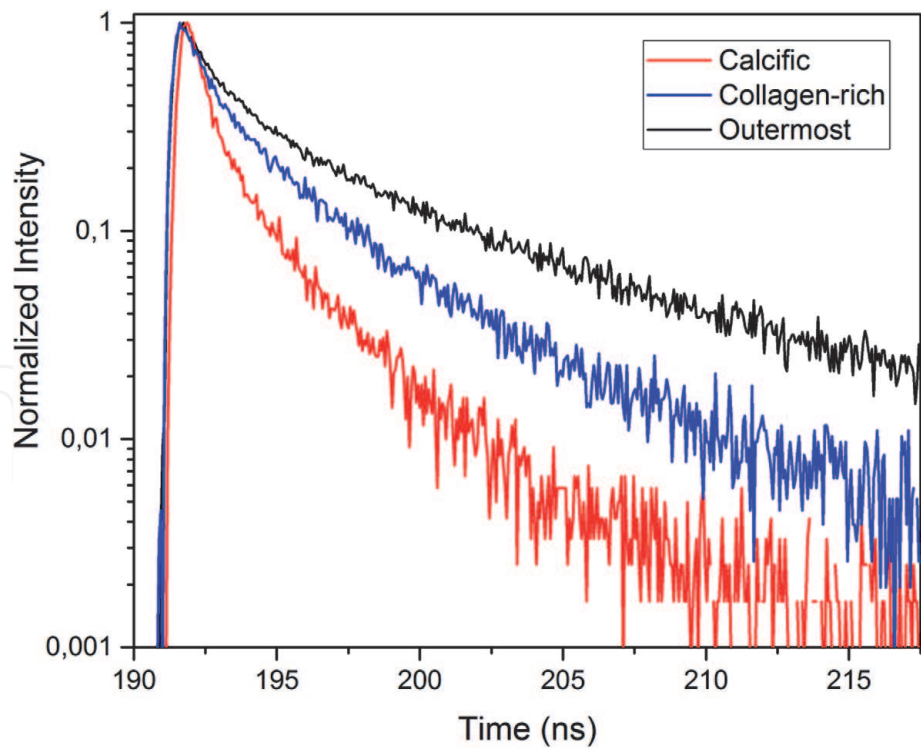


Figure 6.
Fluorescence decay curves of the CdTe/CdS QDs on regions of 1, 3, and 4 on a plaque sample.

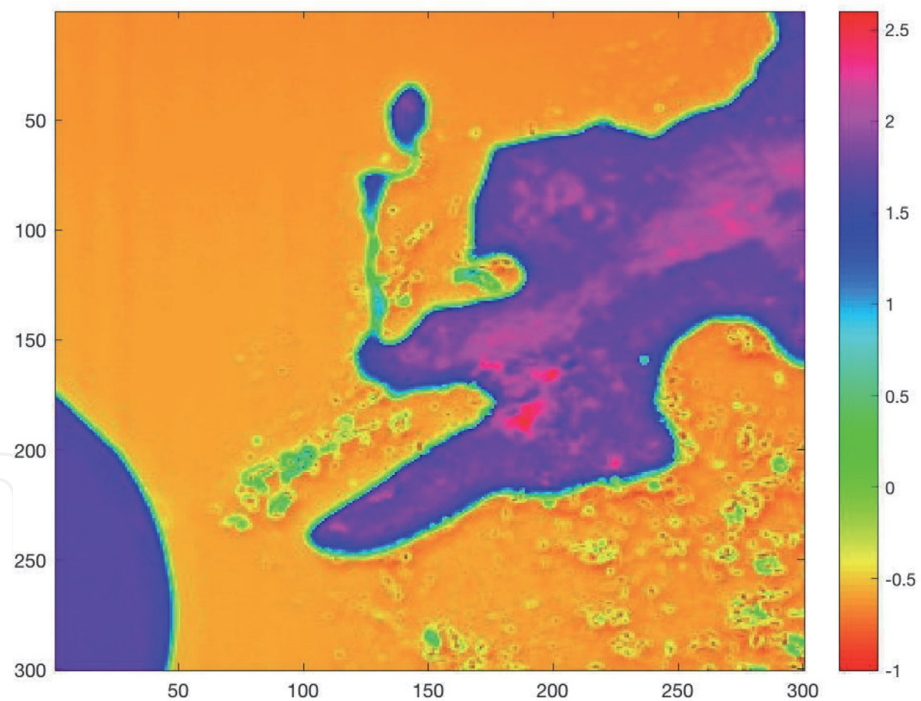


Figure 7.
Acoustic impedance map of a severely calcific plaque sample obtained with acoustic impedance mode of SAM. The scanning area is 4.8 mm x 4.8 mm.

section on the polystyrene substrate. The acoustic impedance distribution indicates different acoustic properties due to the variation of elasticity within the atherosclerotic plaques. The acoustic impedance is determined to be less than 2 MRayl for the collagen-rich areas and greater than 2 MRayl for the calcified areas.

SAM in acoustic impedance mode measures the acoustic impedance of the target by comparing the reflected signal from the tissue with the one from the reference. The reflected signal from the reference is

$$S_{ref} = \frac{Z_{ref} - Z_{sub}}{Z_{ref} + Z_{sub}} S_0 \tag{5}$$

where S_0 is the signal generated by the transducer of SAM, Z_{ref} is the reference's acoustic impedance (1.50 MRayl), and Z_{sub} is the substrate's acoustic impedance (2.37 MRayl). The signal reflected by the target is

$$S_{target} = \frac{Z_{target} - Z_{sub}}{Z_{target} + Z_{sub}} S_0 \tag{6}$$

Consequently, the target's acoustic impedance is calculated as

$$Z_{target} = \frac{1 + \frac{S_{target}}{S_0}}{1 - \frac{S_{target}}{S_0}} Z_{sub} \tag{7}$$

2.5 Photoacoustic microscopy (PAM)

An optically resolved setting (OR-PAM), where focused spot-size on the sample determines the resolution of the system, is successful in imaging the atherosclerotic plaques, as can be seen in **Figure 8**. Calcific regions with greater acoustic impedance values (**Figure 8b**) can also be discriminated by PAM (**Figure 8c**).

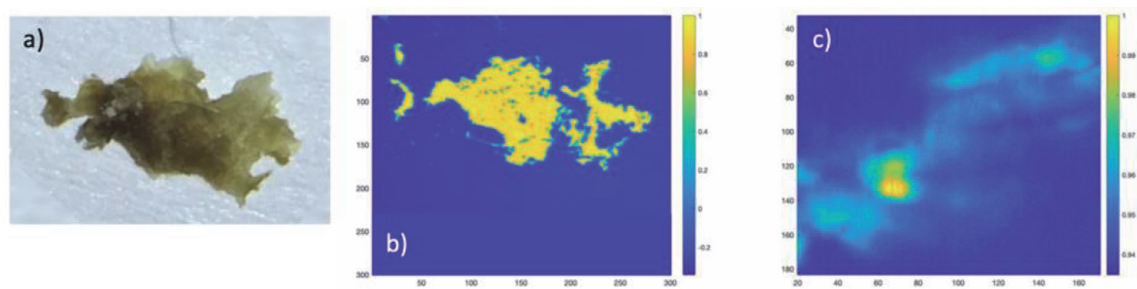


Figure 8.
(a) Digital image, (b) normalized acoustic impedance map, and (c) photoacoustic image of the sample.

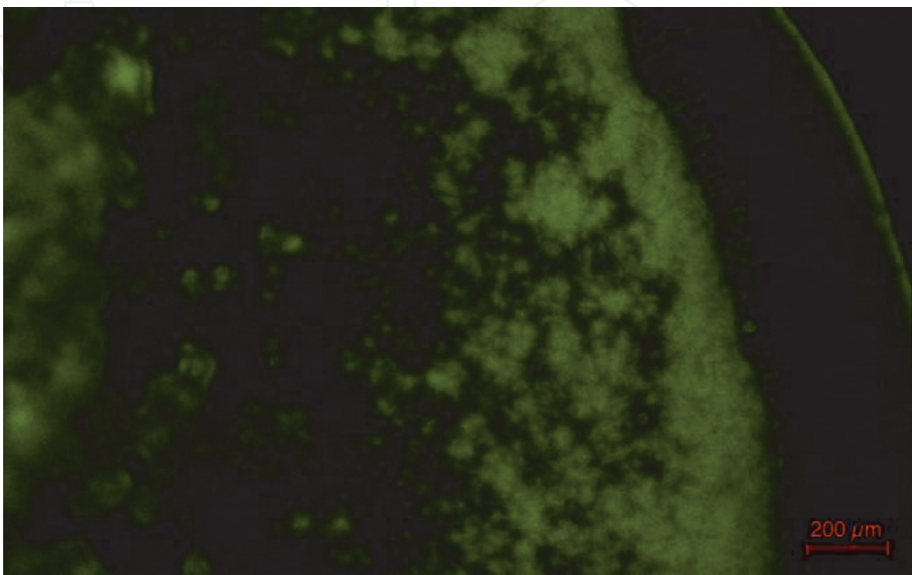


Figure 9.
Photoluminescence image of CdTe/CdS QDs excited with 430 nm. Scale bar is 200 = μm.

3. Quantum dots (QDs)

Photostable QDs are widely used in imaging systems. The photoluminescence image of CdTe/CdS QD aggregates excited with 430 nm is obtained by an inverted fluorescence microscope, as shown in **Figure 9**. The excellent fluorescence intensity with light stability of QDs makes them favorable as diagnostic agents. Use of CdTe/CdS QDs in TRFS experiments of this study reveals their potential in biomedical applications.

4. Conclusion

Here, we discuss the abilities of the imaging modalities on the determination of plaque components of atherosclerotic fibrocalcific plaques. The determination of collagen and calcification within the plaques is done successfully. Micro-CT, SEM, and PAM monitors the microcalcifications. EDS provides elemental distribution within plaques, while TRFS provides information about the molecular environment of the plaques by measuring the lifetime values of CdTe/CdS QDs. SAM provides micrometer resolution in morphology and also mechanical information about the samples. Acoustic impedance maps of the samples show clearly different values in collagen-rich and calcified regions. Consequently, SAM seems predominant over other modalities since SAM is capable of acquiring morphological and chemical information about the plaques simultaneously and usable in clinics. However, for in vivo studies, first, an intravascular SAM probe, similar to intravascular ultrasound (IVUS) probe, has to be developed.

Acknowledgements

Micro-CT experiments were performed in 3D Medical and Industrial Design Laboratory in Istanbul University. SEM-EDS experiments were performed in Nanotechnology Research and Application Center in Sabancı University. TRFS experiments were performed in Photonics Laboratory in Bogazici University. SAM and PAM experiments were performed in Biological and Medical Laboratory in Bogazici University.

Conflict of interest

The author declares no conflict of interest.

Notes/thanks/other declaration

I want to thank all the colleagues who helped me to discuss the characterization techniques mentioned here. Thanks to Leyla Sener Turker for micro-CT experiments. Thanks to Meltem Sezen for SEM-EDS experiments. Thanks to M. Naci Inci for TRFS experiments. Many thanks to M. Burcin Unlu for allowing me to use all of the facilities of Biological and Medical Laboratory not only for SAM and PAM experiments but also for many other research topics.

Appendices and nomenclature


Notation	Definition	Location first used
I	Fluorescence intensity	Eq. (1)
A	Decay amplitude	Eq. (1)
τ	Fluorescence lifetime	Eq. (1)
f	Fractional impact	Eq. (2)
Z_{ref}	Reference's acoustic impedance	Eq. (5)
Z_{sub}	Substrate's acoustic impedance	Eq. (5)
S_{ref}	Reflected signal from the reference	Eq. (5)
S_0	Signal generated by the transducer	Eq. (5)

Author details

Bukem Tanoren Bilen
Department of Physics, Bogazici University, Istanbul, Turkey

*Address all correspondence to: bukem.bilen1@boun.edu.tr

IntechOpen

© 2019 The Author(s). Licensee IntechOpen. This chapter is distributed under the terms of the Creative Commons Attribution License (<http://creativecommons.org/licenses/by/3.0>), which permits unrestricted use, distribution, and reproduction in any medium, provided the original work is properly cited. 

References

- [1] Virmani R, Kolodgie FD, Burke AP, Farb A, Schwartz SM. Lessons from sudden coronary death: A comprehensive morphological classification scheme for atherosclerotic lesions. *Arteriosclerosis Thrombosis and Vascular Biology*. 2000;**20**:1262-1275
- [2] Bentzon JF, Otsuka F, Virmani R, Falk E. Mechanisms of plaque formation and rupture. *Circulation Research*. 2014;**114**:1852-1866
- [3] Insull W. The pathology of atherosclerosis: Plaque development and plaque responses to medical treatment. *The American Journal of Medicine*. 2009;**122**(1A):s3-s14
- [4] Bailey G, Meadows J, Morrison AR. Imaging atherosclerotic plaque calcification: Translating biology. *The American Journal of Medicine*. 2016;**18**(8):51
- [5] Vengrenyuk Y, Carlier S, Xanthos S, Cardoso L, Ganatos P, Virmani R, et al. A hypothesis for vulnerable plaque rupture due to stress-induced debonding around cellular microcalcifications in thin fibrous caps. *Proceedings of the National Academy of Sciences*. 2006;**103**(40):14678-14683
- [6] Shanahan CM. Inflammation ushers in calcification. *Circulation*. 2007;**116**:12782-12785
- [7] Aikawa E, Nahrendorf M, Figueiredo JL, Swirski FK, Shtatland T, Kohler RH, et al. Osteogenesis associates with inflammation in early-stage atherosclerosis evaluated by molecular imaging in vivo. *Circulation*. 2007;**116**:12841-12850
- [8] Hjortnaes J, New SEP, Aikawa E. Visualizing novel concepts of cardiovascular calcification. *Trends in Cardiovascular Medicine*. 2013;**23**(3):71-79
- [9] Van Dessel J, Huang Y, Depypere M, Rubira-Bullen I, Maes F, Jacobs R. A comparative evaluation of cone beam CT and micro-CT on trabecular bone structures in the human mandible. *Dentomaxillofacial Radiology*. 2013;**42**:20130145
- [10] Acar B, Kamburoğlu K, Tatar I, Arıkan V, Çelik H, Yüksel S. Comparison of micro-computerized tomography and cone-beam computerized tomography in the detection of accessory canals in primary molars. *Imaging Science in Dentistry*. 2015;**45**:205-211
- [11] Bauer JS, Link TM, Burghardt A, Henning TD, Mueller D, Majumdar S. Analysis of trabecular bone structure with multidetector spiral computed tomography in a simulated soft-tissue environment. *Calcified Tissue International*. 2007;**80**:366-373
- [12] Rovaris K, Ferreira LM, Sousa TO, Peroni LV, Freitas DQ, Wenzel A, et al. Feasibility of micro-computed tomography to detect and classify proximal caries lesions in vitro. *Dental Research Journal*. 2018;**15**(2):123-129
- [13] Phipps J, Sun Y, Saroufeem R, Hatami N, Fishbein MC, Marcu L. Fluorescence lifetime imaging for the characterization of the biochemical composition of atherosclerotic plaques. *Journal of Biomedical Optics*. 2011;**16**(9):096018
- [14] Phipps JE, Sun Y, Fishbein MC, Marcu L. A fluorescence lifetime imaging classification method to investigate the collagen to lipid ratio in fibrous caps of atherosclerotic plaque. *Lasers in Surgery and Medicine*. 2012;**44**:564-571
- [15] Phipps J, Sun Y, Hatami N, Fishbein MC, Rajaram A, Saroufeem R, et al. Endoscopic fluorescence lifetime

- imaging microscopy (FLIM) images of aortic plaque: an automated classification method. In: Proceedings of SPIE; 23–28 January 2010; San Francisco. SPIE. 2010. p. 754839
- [16] Marcu L. Fluorescence lifetime in cardiovascular diagnostics. *Journal of Biomedical Optics*. 2010;15(1):011106
- [17] Cicchi R, Baria E, Matthaues C, Lange M, Lattermann A, Brehm BR, et al. Non-linear imaging and characterization of atherosclerotic arterial tissue using combined {SHG} and {FLIM} microscopy. *Journal of Biophotonics*. 2015;8(4):347-356
- [18] Jo JA, Park J, Pande P, Shrestha S, Serafino MJ, Jimenez JJR, et al. Simultaneous morphological and biochemical endogeneous optical imaging of atherosclerosis. *Cardiovascular Imaging*. 2015;16:910-918
- [19] Dochow S, Fatakawala H, Phipps JE, Ma D, Bocklitz T, Schmitt M, et al. Comparing Raman and fluorescence lifetime spectroscopy from human atherosclerotic lesions using a bimodal probe. *Journal of Biophotonics*. 2016;9:958-966
- [20] Fatakawala H, Gorpas D, Bishop JW, Bec J, Ma D, Southard JA, et al. Fluorescence lifetime imaging combined with conventional intravascular ultrasound for enhanced assessment of atherosclerotic plaques: An ex vivo study in human coronary arteries. *Journal of Cardiovascular Translational Research*. 2015;8:253-263
- [21] Bec J, Ma DM, Yankelevich DR, Liu J, Ferrier WT, Southard J, et al. Multispectral fluorescence lifetime imaging system for intravascular diagnostics with ultrasound guidance: In vivo validation in swine arteries. *Journal of Biophotonics*. 2014;7(5):281-285
- [22] Kamiyama N, Okomura Y, Kakee A, Hashimoto H. Investigation of ultrasound image processing to improve perceptibility of microcalcifications. *Journal of Medical Ultrasonics*. 2008;35:97-105
- [23] Hui J, Cao Y, Zhang Y, Kole A, Wang P, Yu G, et al. Real-time intravascular photoacoustic-ultrasound imaging of lipid-laden plaque in human coronary artery at 16 frames per second. *Scientific Reports*. 2017;7:1417
- [24] Xu M, Wang L. Photoacoustic imaging in biomedicine. *Review of Scientific Instruments*. 2006;77:041101
- [25] Zhou Y, Yao J, Wang L. Tutorial on photoacoustic tomography. *Journal of Biomedical Optics*. 2016;21:061007-061007
- [26] Miura K, Egawa Y, Moriki T, Mineta H, Harada H, Baba S, et al. Microscopic observation of chemical modification in sections using scanning acoustic microscopy. *Pathology International*. 2015;65(7):355-366
- [27] Y Saijo Y, Filho ES, Sasaki H, Yambe T, Tanaka M, Hozumi N, et al. Ultrasonic tissue characterization of atherosclerosis by a speed-of-sound microscanning system. *IEEE Transactions on Ultrasonics Ferroelectrics and Frequency Control*. 2007;54(8):1571-1577
- [28] Akhtar R, Cruickshank JK, Zhao X, Derby B, Weber T. A pilot study of scanning acoustic microscopy as a tool for measuring arterial stiffness in aortic biopsies. *Artery Research*. 2016;13:1-5
- [29] Y Saijo Y, Hozumi N, Lee C, Nagao M, Kobayashi K, Oakada N, et al. Ultrasonic speed microscopy for imaging of coronary artery. *Ultrasonics*. 2006;44:e51-e55
- [30] Miura K, Katoh H. Structural and histochemical alterations in the aortic valves of elderly patients: A comparative study of aortic stenosis, aortic

regurgitation, and normal valves. *Biomed Research International*. 2016; **2016**:6125204

[31] Brewin MP, Srodon PD, Greenwald SE, Birch MJ. Carotid atherosclerotic plaque characterization by measurement of ultrasound sound speed in vitro at high frequency, 20 MHz. *Ultrasonics*. 2014;**54**:428-441

[32] Saijo Y, Miyakawa T, Sasaki H, Tanaka M, Nitta S. Acoustic properties of aortic aneurysm obtained with scanning acoustic microscopy. *Ultrasonics*. 2004;**42**:695-698

[33] Saijo Y, Ohashi T, Sasaki H, Sato M, Jorgensen CS, Nitta S. Application of scanning acoustic microscopy for assessing stress distribution in atherosclerotic plaque. *Annals of Biomedical Engineering*. 2001;**29**: 1048-1053

[34] Miura K, Nasu H, Yamamoto S. Scanning acoustic microscopy for characterization of neoplastic and inflammatory lesions of lymph nodes. *Scientific Reports*. 2013;**3**:1255

[35] Miura K, Yamamoto S. Pulmonary imaging with a scanning acoustic microscope discriminates speed-of-sound and shows structural characteristics of disease. *Laboratory Investigation*. 2012;**92**:1760-1765

[36] Kobayashi K, Yoshida S, Saijo Y, Hozumi N. Acoustic impedance microscopy for biological tissue characterization. *Ultrasonics*. 2014;**54**: 1922-1928

[37] Hatori K, Saijo Y, Hagiwara Y, Naganuma Y, Igari Kand K, Iikubo M, et al. Acoustic diagnosis device for dentistry. *Interface Oral Health Science*. 2016;**2016**:181-201

[38] Strohm EM, Czarnota GJ, Kolios MC. Quantitative measurements of apoptotic cell properties using acoustic

microscopy. *IEEE Transactions on Ultrasonics Ferroelectrics and Frequency Control*. 2010;**57**(10):2293-2304

[39] Shelke A, Brand S, Kundu T, Bereiter-Hahn J, Blasé C. Mechanical property quantification of endothelial cells using scanning acoustic microscopy. In: *Proceedings of SPIE*; 11–15 March 2012; San Diego, SPIE. 2012. p. 83481T

[40] Brand S, Czarnota GJ, Kolios MC, Weiss EC, Lemor R. Visualization of apoptotic cells using scanning acoustic microscopy and high frequency ultrasound. In: *Proceedings of the IEEE Ultrasonics Symposium 2*; 18-21 September 2005; Rotterdam. IEEE. 2005. pp. 882-885

[41] Masugata H, Mizushige K, Senda S, Kinoshita A, Lu X, Sakamoto H, et al. Tissue characterization of myocardial cells by use of high-frequency acoustic microscopy: Differential myocyte sound speed and its transmural variation in normal, pressure-overload hypertrophic, and amyloid myocardium. *Angiology*. 1999;**50**(10): 837-845

[42] Miura K, Yamamoto S. A scanning acoustic microscope discriminates cancer cells in fluid. *Scientific Reports*. 2015;**5**:15243

[43] Strohm EM, Kolios MC. Quantifying the ultrasonic properties of cells during apoptosis using time resolved acoustic microscopy. In: *IEEE International Ultrasonics Symposium*; 20–23 September 2009; Rome. IEEE. 2009. p. 11208710

[44] Saijo Y, Sasaki H, Sato M, Nitta S, Tanaka M. Visualization of human umbilical vein endothelial cells by acoustic microscopy. *Ultrasonics*. 2000; **38**:396-399

[45] Soon TTK, Chean TW, Yamada H, Takahashi K, Hozumi N, Kobayashi K,

- et al. Effects of anticancer drugs on glioma brain tumor model characterized by acoustic impedance microscopy. *Japanese Journal of Applied Physics*. 2017;**56**:07JF15
- [46] Yoffe AD. Semiconductor quantum dots and related systems: Electronic, optical, luminescence and related properties of low dimensional systems. *Advances in Physics*. 2001;**50**(1):1-208
- [47] Kim H, Beack S, Han S, Shin M, Lee T, Park Y, et al. Multifunctional photonic nanomaterials for diagnostic, therapeutic, and theranostic applications. *Advanced Materials*. 2018;**30**:1701460
- [48] McHugh KJ, Jing L, Behrens AM, Jayawardena SJ, Tang W, Gao M, et al. Biocompatible semiconductor quantum dots as cancer imaging agents. *Advanced Materials*. 2018;**30**:1706356
- [49] Smith AM, Duan H, Mohs AM, Nie S. Bioconjugated quantum dots for in vivomolecular and cellular imaging. *Advanced Drug Delivery Review*. 2008;**60**:1226-1240
- [50] Ohta S, Yamura K, Inasawa S, Yamaguchi Y. Aggregates of silicon quantum dots as a drug carrier: Selective intracellular drug release based on pH-responsive aggregation/dispersion. *Chemical Communications*. 2015;**51**: 6422
- [51] Justin R, Taob K, Román S, Chen D, Xu Y, Geng X, et al. Photoluminescent and superparamagnetic reduced graphene oxide–ironoxide quantum dots for dual-modality imaging, drug delivery and photothermal therapy. *Carbon*. 2016;**97**:54-70
- [52] Zrazhevskiy P, Sena M, Gao X. Designing multifunctional quantum dots for bioimaging, detection, and drug delivery. *Chemical Society Reviews*. 2010;**39**:4326-4354
- [53] Papagiannaros A, Upponi J, Hartner W, Mongayt D, Levchenko T, Torchilin V. Quantum dot loaded immunomicelles for tumor imaging. *BMC Medical Imaging*. 2010;**10**:22
- [54] Hu J, Ortgies DH, Torres RA, Fernandez N, Porto L, Rodriguez EM, et al. Quantum dots emitting in the third biological window as bimodal contrast agents for cardiovascular imaging. *Advanced Functional Materials*. 2017;**27**: 1703276
- [55] Ko NR, Nafiujjaman M, Lee JS, Lim HN, Lee YK, Kwon IK. Graphene quantum dot-based theranostic agents for active targeting of breast cancer. *Royal Society of Chemistry Advances*. 2017;**7**:11420
- [56] Yamazaki R, Ogasawara K, Fujiwara M, Kobayashi K, Saijo Y. Macrophage with gold nanorod visualized by optical-resolution and acoustic-resolution photoacoustic microscopes. In: Conference Proceedings of IEEE Engineering in Medicine and Biology Society; 25–29 August 2015; Milano. IEEE. 2015. pp. 2387-2390
- [57] Ha S, Tripathy S, Carson A, Lavery LL, Zhang H, Agarwal A, et al. Multi-target photoacoustic molecular imaging of cardiovascular inflammatory biomarkers using bioconjugated gold nanorods. In: Proceedings of SPIE; 22–27 January 2011; San Francisco. SPIE. 2011. p. 78991M
- [58] Thakur M, Kumawat MK, Srivastava R. Multifunctional graphene quantum dots for combined photothermal and photodynamic therapy coupled with cancer cell tracking applications. *Royal Society of Chemistry Advances*. 2017;**7**:5251
- [59] Yang K, Zhang S, Zhang G, Sun X, Lee S, Liu Z. Graphene in mice: Ultrahigh In vivo tumor uptake and

efficient photothermal therapy. *Nano Letters*. 2010;**10**:3318-3323

[60] Chong Y, Ma Y, Shen H, Tu X, Zhou X, Xu J, et al. The in vitro and in vivo toxicity of graphene quantum dots. *Biomaterials*. 2014;**35**:5041-5048

[61] Wang H, Revia R, Wang K, Kant RJ, Mu Q, Gai Z, et al. Paramagnetic properties of metal-free boron-doped graphene quantum dots and their application for safe magnetic resonance imaging. *Advanced Materials*. 2017; **29**(11):1605416

[62] Hong H, Chen F, Cai W. Pharmacokinetic issues of imaging with nanoparticles: Focusing on carbon nanotubes and quantum dots. *Molecular Imaging and Biology*. 2013;**15**:507-520

[63] Nguyen KT, Sreejith S, Joseph J, He T, Borah P, Guan EY, et al. Poly (acrylic acid)-capped and dye-loaded graphene oxide-mesoporous silica: A nano-sandwich for two-photon and photoacoustic dual-mode imaging. *Particle and Particle Systems Characterization*. 2014;**31**:1060-1066

[64] Ge J, Jia Q, Liu W, Guo L, Liu Q, Lan M, et al. Red-emissive carbon dots for fluorescent, photoacoustic, and thermal theranostics in living mice. *Advanced Materials*. 2015;**27**:4169-4177